Science Advances
AAAS

advances.sciencemag.org/cgi/content/full/6/30/eaay7170/DC1

Supplementary Materials for

Distortion matrix concept for deep optical imaging in scattering media

Amaury Badon, Victor Barolle, Kristina Irsch, A. Claude Boccara, Mathias Fink, Alexandre Aubry*

*Corresponding author. Email: alexandre.aubry@espci.fr

Published 22 July 2020, *Sci. Adv.* **6**, eaay7170 (2020)
DOI: 10.1126/sciadv.aay7170

This PDF file includes:

Supplementary Materials

S1 Correlations of the reflected and distorted wave-fields in the pupil plane

In this section, we derive the pupil correlations of the $\mathbf{R}$- and $\mathbf{D}$- matrices. Our aim is to provide a theoretical proof of the experimental observation made in Fig.1C2 and 1D2. The distorted wave-fields exhibit correlations over a longer range than the reflected wave-fields in the pupil plane. For sake of analytical tractability but without loss of generality, we will assume in this section: (*i*) a set of fully incoherent input focal spots (*i.e* a strong aberration regime); (*ii*) a field-of-illumination (FOI) contained in a single IP. The main result is the following: While the pupil correlation length r_P of $\mathbf{R}$ scales as the inverse of the FOI size ($r_P \sim \lambda f/\Omega$), the correlation length d_P of $\mathbf{D}$ is inversely proportional to the width δ_{in} of the input PSF ($r_P \sim \lambda f/\delta_{\text{in}}$). The proofs of these two assertions are provided below.

S1.1 Reflection matrix

To investigate the angular correlations of the reflected wave-field, the correlation matrix $\mathbf{B_R} = N_{\text{in}}^{-1}\mathbf{R}\mathbf{R}^\dagger$ should be considered. Using Eq. 2, its coefficients can be expressed as follows:

$$B_R(\mathbf{u}_{\text{out}}, \mathbf{u'}_{\text{out}}) = N_{\text{in}}^{-1} \int_\Omega d\mathbf{r} \int_\Omega d\mathbf{r'} T(\mathbf{u}_{\text{out}}, \mathbf{r}) T^*(\mathbf{u'}_{\text{out}}, \mathbf{r'}) \gamma(\mathbf{r}) \gamma^*(\mathbf{r'}) \sum_{\mathbf{r}_{\text{in}}} H_{\text{in}}(\mathbf{r}, \mathbf{r}_{\text{in}}) H_{\text{in}}^*(\mathbf{r'}, \mathbf{r}_{\text{in}}). \tag{S1}$$

In a strong aberration regime, the input focal spots can be considered as fully incoherent,

$$\langle H_{\text{in}}(\mathbf{r}, \mathbf{r}_{\text{in}}) H_{\text{in}}^*(\mathbf{r'}, \mathbf{r}_{\text{in}}) \rangle = \left\langle |H_{\text{in}}(\mathbf{r}, \mathbf{r}_{\text{in}})|^2 \right\rangle \delta(\mathbf{r} - \mathbf{r'}). \tag{S2}$$

where δ is the Dirac distribution and the symbol $\langle \cdots \rangle$ denotes an ensemble average. In a strong aberration regime, $\mathbf{B_R}$ can be decomposed as the sum of a covariance matrix $\langle \mathbf{B_R} \rangle$ and a perturbation term $\delta\mathbf{B_R}$:

$$\mathbf{B_R} = \langle \mathbf{B_R} \rangle + \delta\mathbf{B_R}, \tag{S3}$$

The correlation matrix $\mathbf{B_R}$ (Eq. S3) should converge towards the covariance matrix $\langle \mathbf{B} \rangle$ for a sufficiently large number $M_R \sim (\Omega/\delta^0_{\text{in}})^2$ of independent speckle grains in the focal plane (Eq.S27). More precisely, the intensity of the perturbation term in Eq.S3, $|\delta \mathbf{B_R}|^2$, scales as the inverse of M_R (*57–59*).

Assuming the convergence of $\mathbf{B_R}$ towards $\langle \mathbf{B_R} \rangle$ ($M_R >> 1$), the correlation coefficients $B_R(\mathbf{u}_{\text{out}}, \mathbf{u'}_{\text{out}})$ (Eq. S1) can be expressed as follows:

$$B_R(\mathbf{u}_{\text{out}}, \mathbf{u'}_{\text{out}}) = N_{\text{in}}^{-1} \int d\mathbf{r} T(\mathbf{u}_{\text{out}}, \mathbf{r}) |\gamma(\mathbf{r})|^2 T^*(\mathbf{u'}_{\text{out}}, \mathbf{r}) \times \sum_{\mathbf{r}_{\text{in}}} \left\langle |H_{\text{in}}(\mathbf{r}, \mathbf{r}_{\text{in}})|^2 \right\rangle, \tag{S4}$$

To go further, an isoplanatic configuration should be considered. On the one hand, this means that the input PSF is invariant by translation:

$$H_{\text{in}}(\mathbf{r}, \mathbf{r}_{\text{in}}) = H_{\text{in}}(\mathbf{r} - \mathbf{r}_{\text{in}}) \tag{S5}$$

On the other hand, the output transmission matrix coefficients $T(\mathbf{u}_{\text{out}}, \mathbf{r})$ can be decomposed as the product of the transmittance $\hat{H}_{\text{out}}(\mathbf{u}_{\text{out}})$ of the aberrating layer and the free-space transmission matrix coefficients $T_0(\mathbf{u}_{\text{out}}, \mathbf{r})$ (Eq.3):

$$T(\mathbf{u}_{\text{out}}, \mathbf{r}) = \hat{H}_{\text{out}}(\mathbf{u}_{\text{out}}) T_0(\mathbf{u}_{\text{out}}, \mathbf{r}). \tag{S6}$$

Injecting these last equations and Eq. 3 into Eq. S4 leads to the following expression for :

$$B_R(\mathbf{u}_{\text{out}}, \mathbf{u'}_{\text{out}}) = I_{\text{in}} \hat{H}_{\text{out}}(\mathbf{u}_{\text{out}}) \hat{H}^*_{\text{out}}(\mathbf{u'}_{\text{out}}) \hat{\gamma}(\mathbf{u'}_{\text{out}} - \mathbf{u}_{\text{out}}) \tag{S7}$$

where

$$I_{\text{in}} = N_{\text{in}}^{-1} \sum_{\mathbf{r}_{\text{in}}} \left\langle |H_{\text{in}}(\mathbf{r} - \mathbf{r}_{\text{in}})|^2 \right\rangle$$

is the mean input PSF intensity and

$$\hat{\gamma}(\mathbf{u}) = \int d\mathbf{r} |\gamma(\mathbf{r})|^2 \exp(-j 2\pi \mathbf{u}.\mathbf{r}/\lambda f)$$

is the 2D Fourier transform of the scattering distribution $|\gamma(\mathbf{r})|^2$ in the focal plane. This quantity, which dictates the correlations displayed by $\mathbf{R}$ in the pupil plane, can be seen as an incoherent structure factor of the object placed in the FOI. The corresponding coherence length r_p scales as

$$r_P \sim \lambda f/\Omega, \tag{S8}$$

The number N_R of independent speckle grains in the reflected wave-field is given by the squared ratio between the output pupil size $\mathcal{D}_{\text{out}} = \lambda f/\delta^0_{\text{out}}$ and the pupil coherence length r_P:

$$N_R \sim (\Omega/\delta^0_{\text{out}})^2 \tag{S9}$$

N_R scales as the number of output resolution cells mapping the object.

These theoretical predictions account for the incoherence of the reflected wave-field shown in Fig. 1C3. This figure plots the auto-correlation function $\mathcal{B}_R(\Delta\mathbf{u})$ of the reflected wave-field in the pupil plane. It is computed by averaging the correlation matrix coefficients $B_R(\mathbf{u}_{\text{out}}, \mathbf{u'}_{\text{out}})$ over couples $(\mathbf{u}_{\text{out}}, \mathbf{u'}_{\text{out}})$ sharing the same relative position $\Delta\mathbf{u} = \mathbf{u}_{\text{out}} - \mathbf{u'}_{\text{out}}$.

S1.2 Distortion matrix

As highlighted by Fig. 1C and demonstrated above, the reflection matrix displays a random feature at the output in the strong aberration regime. Now we will show how the realignment of the reflected wave-fronts in the pupil plane can reveal the angular correlations of the distorted component.

The distortion matrix $\mathbf{D}$ is defined as the Hadamard product between the reflection matrix $\mathbf{R}$ and the reference transmission matrix $\mathbf{T}_0^*$ (Eqs. 4-5). In the isoplanatic limit (Eqs. S5-S6) and using Eq.2, the $\mathbf{D}$-matrix coefficients can be expressed as follows

$$D(\mathbf{u}_{\text{out}}, \mathbf{r}_{\text{in}}) = \hat{H}_{\text{out}}(\mathbf{u}_{\text{out}}) \int d\mathbf{r} T_0(\mathbf{u}_{\text{out}}, \mathbf{r} - \mathbf{r}_{\text{in}}) \gamma(\mathbf{r}) H_{\text{in}}(\mathbf{r} - \mathbf{r}_{\text{in}}). \tag{S10}$$

To investigate the angular correlations between distorted wave-fields, the spatial correlation matrix $\mathbf{B_D} = N_{\text{in}}^{-1}\mathbf{D}\mathbf{D}^{\dagger}$ is investigated. Its coefficients can be expressed as follows:

$$\begin{aligned} B_D(\mathbf{u}_{\text{out}}, \mathbf{u'}_{\text{out}}) &= N_{\text{in}}^{-1}\hat{H}(\mathbf{u}_{\text{out}})\hat{H}^*(\mathbf{u'}_{\text{out}}) \\ &\times \int d\mathbf{r_1} \int d\mathbf{r_2}\gamma(\mathbf{r_1})\gamma^*(\mathbf{r_2}) \\ &\times \sum_{\mathbf{r}_{\text{in}}} H_{\text{in}}(\mathbf{r_1} - \mathbf{r}_{\text{in}})T_0(\mathbf{u}_{\text{out}}, \mathbf{r_1} - \mathbf{r}_{\text{in}})H_{\text{in}}^*(\mathbf{r_2} - \mathbf{r}_{\text{in}})T_0^*(\mathbf{u'}_{\text{out}}, \mathbf{r_2} - \mathbf{r}_{\text{in}}) \end{aligned} \tag{S11}$$

As $\mathbf{B_R}$ (Eq. S3), $\mathbf{B_D}$ can be decomposed as the sum of a covariance matrix $\langle \mathbf{B_D} \rangle$ and a perturbation term $\delta\mathbf{B_D}$ whose intensity decreases with the number $M_D \sim (\Omega/\ell_F)^2$ of independent speckle grains for the distorted wave-field from the focal plane (Eq. S35). For $M_D >> 1$, $\mathbf{B_D}$ converges towards $\langle \mathbf{B_D} \rangle$, such that:

$$\begin{aligned} B_D(\mathbf{u}_{\text{out}}, \mathbf{u'}_{\text{out}}) &= N_{\text{in}}^{-1}\hat{H}(\mathbf{u}_{\text{out}})\hat{H}^*(\mathbf{u'}_{\text{out}}) \\ &\times \int d\mathbf{r_1} \int d\mathbf{r_2}\gamma(\mathbf{r_1})\gamma^*(\mathbf{r_2}) \\ &\times \sum_{\mathbf{r}_{\text{in}}} \langle H_{\text{in}}(\mathbf{r_1} - \mathbf{r}_{\text{in}})H_{\text{in}}^*(\mathbf{r_2} - \mathbf{r}_{\text{in}})\rangle T_0(\mathbf{u}_{\text{out}}, \mathbf{r_1} - \mathbf{r}_{\text{in}})T_0^*(\mathbf{u'}_{\text{out}}, \mathbf{r_2} - \mathbf{r}_{\text{in}}) \end{aligned} \tag{S12}$$

Assuming a strong aberration regime (Eq. S2), the expression of the correlation matrix coefficients $B_D(\mathbf{u}_{\text{out}}, \mathbf{u'}_{\text{out}})$can be simplified as follows

$$B_D(\mathbf{u}_{\text{out}}, \mathbf{u'}_{\text{out}}) = I_0\hat{H}(\mathbf{u}_{\text{out}})\hat{H}^*(\mathbf{u'}_{\text{out}}) \int d\mathbf{r_1}|\gamma(\mathbf{r_1})|^2 \sum_{\mathbf{r'}_{\text{in}}} T_0(\mathbf{u}_{\text{out}}, \mathbf{r'}_{\text{in}})T_0^*(\mathbf{u'}_{\text{out}}, \mathbf{r'}_{\text{in}})\gamma_D(\mathbf{r'}_{\text{in}}) \tag{S13}$$

with $\mathbf{r'}_{\text{in}} = \mathbf{r_1} - \mathbf{r}_{\text{in}}$ and

$$\gamma_D(\mathbf{r'}_{\text{in}}) = \left\langle |H_{\text{in}}(\mathbf{r'}_{\text{in}})|^2 \right\rangle, \tag{S14}$$

the intensity distribution of the virtual source synthesized in the focal plane at the input. Using Eqs. 3 and S6, Eq. S13 can be rewritten as

$$B_D(\mathbf{u}_{\text{out}}, \mathbf{u'}_{\text{out}}) \propto \hat{H}(\mathbf{u}_{\text{out}})\hat{H}^*(\mathbf{u'}_{\text{out}})\hat{\gamma}_D(\mathbf{u'}_{\text{out}} - \mathbf{u}_{\text{out}}) \tag{S15}$$

where $\hat{\gamma}_D(\mathbf{u}) = \sum_{\mathbf{r}} \gamma_D(\mathbf{r}) \exp(-j2\pi \mathbf{u}.\mathbf{r}/\lambda f)$ is a discrete 2D Fourier transform of the scattering distribution $\gamma_D(\mathbf{r})$ in the focal plane. The correlation length d_p of the distorted wave-field in the pupil plane is thus inversely proportional to the spatial extension δ_{in} of the input PSF intensity $|H_{\text{in}}|^2$, such that

$$d_P \sim \lambda f / \delta_{\text{in}}. \tag{S16}$$

The number of independent speckle grains in the distorted wave-field is the squared ratio between the output pupil size $\mathcal{D}_{\text{out}} = \lambda f / \delta^0_{\text{out}}$ and the pupil coherence length d_P:

$$N_D \sim (\delta_{\text{in}} / \delta^0_{\text{out}})^2 \tag{S17}$$

N_D scales as the number of output resolution cells mapping the input PSF.

As δ_{in} is smaller than the FOI dimension Ω, d_P/N_D are larger/smaller than r_P/N_R (Eqs. S8-S9), respectively. This highlights the enhancement of the far-field correlations in $\mathbf{D}$ shown in Fig. 1D3. This figure plots the auto-correlation function $\mathcal{B}_D(\Delta\mathbf{u})$ of the distorted wave-field in the pupil plane. $\mathcal{B}_D(\Delta\mathbf{u})$ is computed by averaging the correlation matrix coefficients $B_D(\mathbf{u}_{\text{out}}, \mathbf{u'}_{\text{out}})$ over couples $(\mathbf{u}_{\text{out}}, \mathbf{u'}_{\text{out}})$ of common relative position $\Delta\mathbf{u} = \mathbf{u}_{\text{out}} - \mathbf{u'}_{\text{out}}$.

S2 Spatial correlations of the reflected and distorted wave-fields

In this section, we derive the input correlations of the matrices $\mathbf{R}$ and $\mathbf{D}$. Our aim is to provide a theoretical proof of the experimental observation made in Fig.1C2 and 1D2. As seen previously in the pupil plane, the distorted wave-fields reveal spatial correlations in the focal plane that were originally hidden in the recorded wave-fields. Unlike the previous section, we derive a general expression for the input correlation matrices beyond the isoplanatic limit. The main result is the following: While the correlation length r_F of the reflected wave-field in the focal

plane is restricted to the input diffraction limit resolution δ^0_{in}, the correlation length d_F of $\mathbf{D}$ in the focal plane corresponds to the isoplanatic length ℓ_c.

S2.1 Reflection matrix

To investigate the spatial correlations of the reflected wave-field, the correlation matrix $\mathbf{C_R} = N_{\text{out}}^{-1}\mathbf{R}^\dagger\mathbf{R}$ should this time be considered. Unlike in the previous section, the isoplanatic assumption is here not made. Using Eq. 2, the coefficients of $\mathbf{C_R}$ can be expressed as follows:

$$C_R(\mathbf{r}_{\text{in}}, \mathbf{r'}_{\text{in}}) = N_{\text{out}}^{-1} \int d\mathbf{r} \int d\mathbf{r'} \gamma(\mathbf{r})\gamma^*(\mathbf{r'}) H_{\text{in}}(\mathbf{r}, \mathbf{r}_{\text{in}}) H^*_{\text{in}}(\mathbf{r'}, \mathbf{r'}_{\text{in}}) \sum_{\mathbf{u}_{\text{out}}} T(\mathbf{u}_{\text{out}}, \mathbf{r}) T^*(\mathbf{u}_{\text{out}}, \mathbf{r'}) \tag{S18}$$

As correlation matrices in the pupil plane, $\mathbf{C_R}$ converges towards the covariance matrix $\langle \mathbf{C_R} \rangle$ for a large number $N_R \sim (\Omega/\delta^0_{\text{out}})^2$ of independent speckle grains for the reflected wave-field in the pupil plane (Eq. S27). For $N_R >> 1$, the coefficients of $\mathbf{C_R}$ are given by:

$$C_R(\mathbf{r}_{\text{in}}, \mathbf{r'}_{\text{in}}) = N_{\text{out}}^{-1} \int d\mathbf{r} \int d\mathbf{r'} \gamma(\mathbf{r})\gamma^*(\mathbf{r'}) H_{\text{in}}(\mathbf{r}, \mathbf{r}_{\text{in}}) H^*_{\text{in}}(\mathbf{r'}, \mathbf{r'}_{\text{in}}) \sum_{\mathbf{u}_{\text{out}}} \langle T(\mathbf{u}_{\text{out}}, \mathbf{r}) T^*(\mathbf{u}_{\text{out}}, \mathbf{r'}) \rangle \tag{S19}$$

The mean correlation term $\langle T(\mathbf{u}_{\text{out}}, \mathbf{r}) T^*(\mathbf{u}_{\text{out}}, \mathbf{r'}) \rangle$ can be developed by writing the transmission matrix as a Hadamard product between the free-space transmission matrix $\mathbf{T_0}$ and an aberration matrix $\mathbf{H}_{\text{out}}$, such that

$$T(\mathbf{u}_{\text{out}}, \mathbf{r}) = \hat{H}_{\text{out}}(\mathbf{u}_{\text{out}}, \mathbf{r}) T_0(\mathbf{u}_{\text{out}}, \mathbf{r}).$$

It comes

$$\begin{aligned} \langle T(\mathbf{u}_{\text{out}}, \mathbf{r}) T^*(\mathbf{u}_{\text{out}}, \mathbf{r'}) \rangle &= \left\langle \hat{H}_{\text{out}}(\mathbf{u}_{\text{out}}, \mathbf{r}) \hat{H}^*_{\text{out}}(\mathbf{u}_{\text{out}}, \mathbf{r'}) \right\rangle T_0(\mathbf{u}_{\text{out}}, \mathbf{r}) T_0^*(\mathbf{u}_{\text{out}}, \mathbf{r'}) \quad \text{(S20)} \\ &= F(\mathbf{r}, \mathbf{r'}) \left\langle \left| \hat{H}_{\text{out}}(\mathbf{u}_{\text{out}}, \mathbf{r}) \right|^2 \right\rangle T_0(\mathbf{u}_{\text{out}}, \mathbf{r}) T_0^*(\mathbf{u}_{\text{out}}, \mathbf{r'}). \quad \text{(S21)} \end{aligned}$$

The correlation function,

$$F(\mathbf{r}, \mathbf{r'}) = \left\langle \hat{H}_{\text{out}}(\mathbf{u}_{\text{out}}, \mathbf{r}) \hat{H}^*_{\text{out}}(\mathbf{u}_{\text{out}}, \mathbf{r'}) \right\rangle / \left\langle \left| \hat{H}_{\text{out}}(\mathbf{u}_{\text{out}}, \mathbf{r}) \right|^2 \right\rangle, \tag{S22}$$

describes the spatial correlation of the aberration matrix $\hat{\mathbf{H}}_{\text{out}}$ in the focal plane. Its support is directly related to ℓ_c, the IP size. For sake of simplicity but without lack of generality, we assume that the aberrating layer does not attenuate the wave-field:

$$\left\langle \left| \hat{H}_{\text{out}}(\mathbf{u}_{\text{out}}, \mathbf{r}) \right|^2 \right\rangle = 1. \tag{S23}$$

Using Eq. S21, the sum over $\mathbf{u}_{\text{out}}$ into Eq. S19 can then be rewritten as:

$$N_{\text{out}}^{-1} \sum_{\mathbf{u}_{\text{out}}} \langle T(\mathbf{u}_{\text{out}}, \mathbf{r}) T^*(\mathbf{u}_{\text{out}}, \mathbf{r}') \rangle = F(\mathbf{r}, \mathbf{r}') \sum_{\mathbf{u}_{\text{out}}} T_0(\mathbf{u}_{\text{out}}, \mathbf{r}) T_0^*(\mathbf{u}_{\text{out}}, \mathbf{r}') \tag{S24}$$

Injecting the expression of the coefficients $T_0(\mathbf{u}_{\text{out}}, \mathbf{r}_{\text{in}})$ (Eq. 3), it finally comes

$$\begin{aligned} N_{\text{out}}^{-1} \sum_{\mathbf{u}_{\text{out}}} \langle T(\mathbf{u}_{\text{out}}, \mathbf{r}) T^*(\mathbf{u}_{\text{out}}, \mathbf{r}') \rangle &= F(\mathbf{r}, \mathbf{r}') \sum_{\mathbf{u}_{\text{out}}} \exp\left(i \frac{2\pi}{\lambda f} \mathbf{u}_{\text{out}} . (\mathbf{r} - \mathbf{r}') \right) \\ &= \delta(\mathbf{r} - \mathbf{r}') \end{aligned} \tag{S25}$$

The physical meaning of this last equation is that two virtual sources located at points $\mathbf{r}$ and $\mathbf{r}'$ in the focal plane give rise to uncorrelated wave-fields in the pupil plane. Injecting this last relation into Eq. S19 leads to the following expression for $C_R(\mathbf{r}_{\text{in}}, \mathbf{r'}_{\text{in}})$

$$C_R(\mathbf{r}_{\text{in}}, \mathbf{r'}_{\text{in}}) = \int d\mathbf{r} |\gamma(\mathbf{r})|^2 H_{\text{in}}(\mathbf{r}, \mathbf{r}_{\text{in}}) H_{\text{in}}^*(\mathbf{r}, \mathbf{r'}_{\text{in}}) \tag{S26}$$

To go further, a rough approximation is to assume an object of constant reflectivity in intensity: $\langle |\gamma(\mathbf{r})|^2 \rangle = \gamma_0^2$. The correlation length r_F of the reflected wave-field then corresponds to the coherence length of the input focal spots. In the strong aberration regime, r_F thus scales as the input diffraction limit δ_{in}^0. The number M_R of independent speckle grains in the focal plane then correspond to the number of input resolution cells mapping the object:

$$M_R \sim (\Omega / \delta_{\text{in}}^0)^2 \tag{S27}$$

These theoretical derivations account for the spatial incoherence exhibited by the reflected wave-field in Fig. 1C2. This figure plots the auto-correlation function $\mathcal{C}_R(\Delta\mathbf{r})$ of the reflected wave-field in the focal plane. $\mathcal{C}_R(\Delta\mathbf{r})$ is computed by averaging the correlation matrix coefficients $C_R(\mathbf{r}_{\text{in}}, \mathbf{r'}_{\text{in}})$ over couples $(\mathbf{r}_{\text{in}}, \mathbf{r'}_{\text{in}})$ of same relative position $\Delta\mathbf{r} = \mathbf{r}_{\text{in}} - \mathbf{r'}_{\text{in}}$.

S2.2 Distortion matrix

As highlighted by Fig. 1C and demonstrated above, the reflection matrix displays a random feature both at its output and input in the strong aberration regime. Now we will show how the de-scan of the input focal spots in the focal plane reveals the spatial correlations between wave distortions.

In the general case (*i.e* beyond the isoplanatic limit), the $\mathbf{D}$-matrix coefficients can be expressed as follows

$$D(\mathbf{u}_{\text{out}},\mathbf{r}_{\text{in}}) = \int d\mathbf{r}\hat{H}_{\text{out}}(\mathbf{u}_{\text{out}},\mathbf{r})T_0(\mathbf{u}_{\text{out}},\mathbf{r}-\mathbf{r}_{\text{in}})\gamma(\mathbf{r})H_{\text{in}}(\mathbf{r},\mathbf{r}_{\text{in}}) \tag{S28}$$

To investigate the spatial correlations of the distorted wave-field in the pupil plane, the correlation matrix $\mathbf{C_D} = N_{\text{out}}^{-1}\mathbf{D}^\dagger\mathbf{D}$ should be considered. As the other correlation matrices, $\mathbf{C_D}$ can be decomposed as the sum of a covariance matrix $\langle\mathbf{C_D}\rangle$ and a perturbation term $\delta\mathbf{C_D}$ whose intensity is inversely proportional to the number, $N_D = (\delta_{\text{in}}/\delta^0_{\text{out}})^2$, of independent pupil speckle grains in the distorted wave-field (Eq. S17).

For $N_D >> 1$, $\mathbf{C_D}$ is shown to converge towards the covariance matrix $\langle\mathbf{C_D}\rangle$. Its coefficients can then be expressed as follows:

$$\begin{aligned} C_D(\mathbf{r}_{\text{in}},\mathbf{r'}_{\text{in}}) &= N_{\text{out}}^{-1}\int d\mathbf{r_1}\int d\mathbf{r_2} H_{\text{in}}(\mathbf{r_1},\mathbf{r}_{\text{in}})H^*_{\text{in}}(\mathbf{r_2},\mathbf{r'}_{\text{in}})\gamma(\mathbf{r_1})\gamma^*(\mathbf{r_2}) \\ &\quad\times\sum_{\mathbf{u}_{\text{out}}}\langle\hat{H}_{\text{out}}(\mathbf{u}_{\text{out}},\mathbf{r_1})\hat{H}^*_{\text{out}}(\mathbf{u}_{\text{out}},\mathbf{r_2})\rangle T_0(\mathbf{u}_{\text{out}},\mathbf{r_1}-\mathbf{r}_{\text{in}})T_0^*(\mathbf{u}_{\text{out}},\mathbf{r_2}-\mathbf{r'}_{\text{in}}) \end{aligned} \tag{S29}$$

Using Eqs. 3, 14 and S23, the sum over $\mathbf{u}_{\text{out}}$ in Eq. S29 can be simplified as follows:

$$\begin{aligned} &N_{\text{out}}^{-1}\sum_{\mathbf{u}_{\text{out}}}\langle\hat{H}_{\text{out}}(\mathbf{u}_{\text{out}},\mathbf{r_1})\hat{H}^*_{\text{out}}(\mathbf{u}_{\text{out}},\mathbf{r_2})\rangle T_0(\mathbf{u}_{\text{out}},\mathbf{r_1}-\mathbf{r}_{\text{in}})T_0^*(\mathbf{u}_{\text{out}},\mathbf{r_2}-\mathbf{r'}_{\text{in}}) \\ &\quad= F(\mathbf{r_1},\mathbf{r_2})\sum_{\mathbf{u}_{\text{out}}}\exp\left(i\frac{2\pi}{\lambda f}\mathbf{u}_{\text{out}}.(\mathbf{r_1}-\mathbf{r}_{\text{in}}-\mathbf{r_2}+\mathbf{r'}_{\text{in}})\right) \\ &\quad= F(\mathbf{r_1},\mathbf{r_2})\delta(\mathbf{r_1}-\mathbf{r}_{\text{in}}-\mathbf{r_2}+\mathbf{r'}_{\text{in}}) \end{aligned} \tag{S30}$$

If the statistical properties of the scattering medium are invariant by translation, then $F(\mathbf{r_1}, \mathbf{r_2}) = F(||\mathbf{r_1} - \mathbf{r_2}||)$. The spatial extension of the function F directly yields the isoplanatic length ℓ_c. The injection of Eq. S30 into Eq. S29 yields

$$C_D(\mathbf{r}_{\text{in}}, \mathbf{r'}_{\text{in}}) = F(\Delta r) \int d\mathbf{r} \gamma(\mathbf{r}) \gamma^*(\mathbf{r} - \Delta\mathbf{r}) H_{\text{in}}(\mathbf{r}, \mathbf{r}_{\text{in}}) H^*_{\text{in}}(\mathbf{r} - \Delta\mathbf{r}, \mathbf{r'}_{\text{in}}). \tag{S31}$$

with $\Delta\mathbf{r} = \mathbf{r}_{\text{in}} - \mathbf{r'}_{\text{in}}$ and $\Delta r = |\mathbf{r}_{\text{in}} - \mathbf{r'}_{\text{in}}|$. The factor $F(\Delta r)$ requires that the correlation coefficients $C_D(\mathbf{r}_{\text{in}}, \mathbf{r'}_{\text{in}})$ cancel for points belonging to different IPs. The input PSFs can thus be considered as locally invariant by translation, such that $H_{\text{in}}(\mathbf{r} - \mathbf{r}_{\text{in}} + \mathbf{r'}_{\text{in}}, \mathbf{r'}_{\text{in}}) \simeq H_{\text{in}}(\mathbf{r} - \mathbf{r}_{\text{in}})$. Equation S31 simplifies into

$$C_D(\mathbf{r}_{\text{in}}, \mathbf{r'}_{\text{in}}) \propto F(\Delta r) \int d\mathbf{r} \gamma(\mathbf{r}) \gamma^*(\mathbf{r} - \Delta\mathbf{r}) |H_{\text{in}}(\mathbf{r}, \mathbf{r}_{\text{in}})|^2, \tag{S32}$$

To go further, we can assume that the width of the input focusing beam δ_{in} is larger than the characteristic fluctuation length ℓ_γ of the sample reflectivity:

$$C_D(\mathbf{r}_{\text{in}}, \mathbf{r'}_{\text{in}}) \sim F(\Delta r)(\gamma * \gamma)(\Delta r). \tag{S33}$$

where the symbol $*$ stands for the correlation product. Depending on the experimental conditions, the coherence length d_F of the distorted wave-field can correspond to the correlation length ℓ_γ of the object's reflectivity or the isoplanatic length ℓ_c associated with the aberrating layer

$$d_F = \min\{\ell_c, \ell_\gamma\} \tag{S34}$$

d_F is thus always larger than the coherence length $r_F \sim \delta^0_{\text{in}}$ of the incoherent reflected wave-field (Eq. S15). The number M_D of independent focal speckle grains for the distorted wave-field is given by

$$M_D = (\Omega/\ell_c)^2 \tag{S35}$$

If $\ell_\gamma > \ell_c$, this number M_D coincides with the number $(\Omega/\ell_c)^2$ of IPs contained by the object.

These theoretical predictions confirm the experimental observations highlighted by Fig. 1. Spatial correlations are drastically enhanced between the input entries of $\mathbf{D}$ (Fig. 1D2) compared to $\mathbf{R}$ (Fig. 1C2). Figure 1D2 plots the auto-correlation function $\mathcal{C}_D(\Delta\mathbf{r})$ of the distorted wave-field in the focal plane. This quantity is calculated by averaging the correlation matrix coefficients $C_D(\mathbf{r}_{\rm in}, \mathbf{r'}_{\rm in})$ over couples $(\mathbf{r}_{\rm in}, \mathbf{r'}_{\rm in})$ sharing the same relative position $\Delta\mathbf{r} = \mathbf{r}_{\rm in} - \mathbf{r'}_{\rm in}$.

Now, we show how the long-range correlations exhibited by $\mathbf{D}$ can be leveraged for overcoming the aberrations and retrieving an image of the object with a resolution close to the diffraction limit.

S3 Singular value decomposition of the distortion matrix

To take advantage of the correlations exhibited by the matrix $\mathbf{D}$, its SVD (Eq. 6) is shown to be an essential tool. It enables a decomposition of the FOI into IMs and an estimation of the transmission matrix $\mathbf{T}$ between the CCD surface and the focal plane. To provide a theoretical proof of this claim, the previous study of the correlation matrices $\mathbf{B_D}$ and $\mathbf{C_D}$ will be helpful. Their eigenvalue decomposition actually dictates the SVD of $\mathbf{D}$. Correlations in the focal plane are shown to predominate in the experiments depicted in the accompanying paper, but also, more generally, in optical microscopy. Strikingly, an exchange of role is noticed between the medium's reflectivity and the input PSF in the $\mathbf{D}$-matrix compared to the original $\mathbf{R}$-matrix. While the first singular vector of $\mathbf{R}$ yields the input PSF for a point-like reflector (*26, 60*), the first singular vector of $\mathbf{D}$ directly yields the sample reflectivity for a point-like input focusing beam in an isoplanatic configuration. Beyond this analogy made between $\mathbf{R}$ and $\mathbf{D}$ in this asymptotic limit, a theoretical proof is then provided in the general case. We show how: (*i*) the SVD of $\mathbf{D}$ allows a decomposition of the FOI into a set of IMs $\mathbf{V_p}$; (*ii*) a coherent combination of the output eigenvectors $\mathbf{U_p}$ can lead to an estimator of the transmission matrix $\mathbf{T}$.

S3.1 Eigenvalue decomposition of the correlation matrices

The SVD of $\mathbf{D}$ (Eq. 6) can be directly deduced from the eigenvalue decompositions of its correlation matrices $\mathbf{B_D}$ and $\mathbf{C_D}$. The latter ones can actually be written as follows

$$\mathbf{B_D} = \mathbf{U}\boldsymbol{\Sigma}^2\mathbf{U}^\dagger \tag{S36}$$

and

$$\mathbf{C_D} = \mathbf{V}\boldsymbol{\Sigma}^2\mathbf{V}^\dagger. \tag{S37}$$

or, in terms of matrix coefficients,

$$B_D(\mathbf{u}_{\text{out}}, \mathbf{u'}_{\text{out}}) = \sum_{p=1}^{N_{\text{in}}} \sigma_p^2 U_p(\mathbf{u}_{\text{out}}) U_p^*(\mathbf{u'}_{\text{out}}). \tag{S38}$$

and

$$C_D(\mathbf{r}_{\text{in}}, \mathbf{r'}_{\text{in}}) = \sum_{p=1}^{N_{\text{in}}} \sigma_p^2 V_p(\mathbf{r}_{\text{in}}) V_p^*(\mathbf{r'}_{\text{in}}). \tag{S39}$$

The eigenvalues of $\mathbf{B_D}$ and $\mathbf{C_D}$ are the square of the singular values σ_p; their eigenvectors, $\mathbf{U_p}$ and $\mathbf{V_p}$, are the output and input singular vectors, respectively. The SVD of $\mathbf{D}$ is dictated either by the correlations between its lines or columns. To know which ones dominate over the other, the analytical expressions of the correlation matrices, $\mathbf{B_D}$ and $\mathbf{C_D}$, should be investigated (see Eqs. S15 and S33).

If the reflectivity of the object was fully random, *i.e* $\langle \gamma(\mathbf{r}) * \gamma(\mathbf{r}) \rangle = \delta(\mathbf{r})$, the correlation matrix $\mathbf{C_D}$ (Eq. S33) would be diagonal. This means that the columns of $\mathbf{D}$ would be fully uncorrelated. On the contrary, output correlations would subsist in $\mathbf{D}$ as they only depend on the spatial extension of the input focal spot (Eq. S16). In this random speckle regime, the SVD of $\mathbf{D}$ is dominated by its correlations in the pupil plane and the analysis of $\mathbf{D}$ should rather be restricted to a FOI containing a single IP. This regime has been recently investigated in medical ultrasound imaging (*51*) where scattering is often due to a random distribution of unresolved scatterers.

In optical microscopy, biological tissues induce a strong forward scattering: The involved scatterers display a characteristic length ℓ_γ larger than the wavelength. The auto-correlation of the sample reflectivity can span over several IPs especially at large depths. In this forward scattering regime, correlations of the distorted wave-field in the focal plane may dominate over its far-field correlations.

To know if this is the case, one can compare the number of independent speckle grains, N_D and M_D, in the pupil and focal planes, respectively. The correlation degree in each plane is actually inversely proportional to this number. Correlations in the focal plane will thus dominate if $N_D > M_D$. The latter condition is fulfilled in a strong aberration regime for which the number of output resolution cells mapping each aberrated focal spot, $N_D = (\delta_{\text{in}}/\delta^0_{\text{out}})^2$, is larger than the number of IPs mapping the object surface, $M_D = (\Omega/\ell_c)^2$. This condition is checked in the experiments of the accompanying paper. For instance, in the experiment depicted in Fig. 4, $N_D \sim 500$ while $M_D \sim 10$.

S3.2 Analogy with iterative time reversal

Now that the conditions for a domination of correlations in the focal plane have been derived, we now study the singular vectors of $\mathbf{D}$. To that aim, an analogy with iterative time reversal is first explored to give a physical intuition of the SVD of $\mathbf{D}$.

If we compare the analytical expressions of the correlation matrices $\mathbf{C_R}$ (Eq. S13) and $\mathbf{C_D}$ (Eq. S31), we can notice an exchange of the role between the medium reflectivity γ and the input PSF H_{in}. While $\mathbf{C_R}$ corresponds to a static object scanned by a moving illuminating beam (Fig.2A), $\mathbf{C_D}$ corresponds to a static focused beam illuminating a moving object (Fig.2B). In the isoplanatic limit, the distortion matrix $\mathbf{D}$ (Eq. S31) is thus equivalent to a virtual reflection matrix associated with: (*i*) a coherent reflector of scattering distribution $|H_{\text{in}}(\mathbf{r})|^2$ (located on the optical axis and at the focal plane); (*ii*) a virtual focusing beam associated with the PSF $\gamma(\mathbf{r}_{\text{in}} +$

$\mathbf{r}$). As shown by iterative time reversal experiments (*60,61*), the reflection matrix is of rank 1 for a point-like scatterer, and its first input singular vector $\mathbf{V_1}$ shall directly yield the virtual input PSF (*27*). By analogy, for a point-like input focusing beam, the $\mathbf{D}$-matrix shall be also of rank 1 and its first input singular vector $\mathbf{V_1}$ shall directly provide the medium reflectivity $\gamma(\mathbf{r}_{\rm in})$. Interestingly, the SVD of $\mathbf{D}$ should therefore unscramble aberrations and sample reflectivity. However, this qualitative analysis has been made under strong hypotheses: the isoplanatic limit and a point-like input focusing beam. In the following, we make the problem more complex by first going beyond the isoplanatic limit and then by considering the finite size of the input focusing beams.

S3.3 Isoplanatic modes

Let us first assume a point-like input focusing beam, $H_{\rm in}(\mathbf{r},\mathbf{r}_{\rm in}) = |H_{\rm in}(\mathbf{r}_{\rm in},\mathbf{r}_{\rm in})|^2\delta(\mathbf{r}-\mathbf{r}_{\rm in})$, beyond the isoplanatic limit. Equation S31 becomes

$$C_D(\mathbf{r}_{\rm in},\mathbf{r'}_{\rm in}) \propto F(\Delta r)\gamma(\mathbf{r}_{\rm in})\gamma^*(\mathbf{r'}_{\rm in})H_{\rm in}(\mathbf{r}_{\rm in},\mathbf{r}_{\rm in})H^*_{\rm in}(\mathbf{r'}_{\rm in},\mathbf{r'}_{\rm in}). \tag{S40}$$

A full-field intensity image $\mathcal{F}(\mathbf{r}_{\rm in})$ of the sample reflectivity can be retrieved by considering the diagonal of $\mathbf{C_D}$:

$$\mathcal{F}(\mathbf{r}_{\rm in}) = C_D(\mathbf{r}_{\rm in},\mathbf{r}_{\rm in}) = |\gamma(\mathbf{r}_{\rm in})|^2|H_{\rm in}(\mathbf{r}_{\rm in},\mathbf{r}_{\rm in})|^2 \tag{S41}$$

$\mathcal{F}(\mathbf{r}_{\rm in})$ can be a satisfying estimator of the sample reflectivity, $|\gamma(\mathbf{r}_{\rm in})|^2$. However, the input focusing beam intensity $H_{\rm in}(\mathbf{r}_{\rm in},\mathbf{r}_{\rm in})$ pollutes the full-field image. The latter term can be detrimental to imaging since it gives rise to a fluctuating contrast across the focal plane. Moreover, experimental noise and diffusive multiple scattering can still degrade the image. At last, we may want to have access to the amplitude and phase of the reflectivity rather than only its square norm. For all these reasons, the singular value decomposition of $\mathbf{D}$ (Eq.6), or equivalently, the eigenvalue decomposition of $\mathbf{C_D}$(Eq.S39) is decisive. In the general case, the correlation

function $F(\Delta r)$ (Eq. S22) governs the eigenvalue decomposition of $\mathbf{C_D}$. The ratio between the object surface Ω^2 and the isoplanatic area ℓ_c^2 yields the effective rank $M_D = (\Omega/\ell_c)^2$ of $\mathbf{C_D}$. This rank scales as the number of IPs that fit in the object. The input eigenvectors $\mathbf{V_p}$ can be derived by solving a second order Fredholm equation with Hermitian kernel (*42*). An analytical solution can be found for certain analytical form of the correlation function $F(\Delta r)$ (Eq. S22). For instance, a sinc kernel imply 3D prolate spheroïdal eigenfunctions (*43*); a Gaussian covariance function leads to Hermite-Gaussian eigenmodes (*44*); exponential or triangular kernels yields cosine and sine eigenfunctions (*42*). A general trend is that the spatial frequency content of the eigenvectors increases with their rank.

The identification of Eqs. S39 and S40 leads to the following equality:

$$\sum_{p=1}^{M_D} \sigma_p V_p(\mathbf{r}_{\text{in}}) = H_{\text{in}}(\mathbf{r}_{\text{in}}, \mathbf{r}_{\text{in}})\gamma(\mathbf{r}_{\text{in}}) \tag{S42}$$

A coherent combination of the M_D first eigenvectors $\mathbf{V_p}$ can yield the amplitude and phase of the reflectivity but the result is still polluted by the input illumination beam $H_{\text{in}}(\mathbf{r}_{\text{in}}, \mathbf{r}_{\text{in}})$. In practice, aberrations at the input can be corrected through the same process by exchanging input and output, *i.e* by projecting the data in the pupil plane at the input and in the focal plane at the ouput. In the experiments depicted in the accompanying paper, the sparse illumination scheme makes the input basis incomplete and the spatial sampling insufficient. The image should thus be built from the output to benefit from the excellent resolution with which the field is recorded by the CCD camera. To do so, Eq. S42 can be used to prove that the coherent combination of output singular vectors $\mathbf{U_c} = \sum_{p=1}^{M_D} \mathbf{U_p}$ (Eq. 6) perfectly compensate for the output aberration matrix $\hat{\mathbf{H}}_{\text{out}}$. To that aim, let us apply the transpose conjugate $\mathbf{U_c^\dagger}$ to the output of the matrix $\mathbf{D}$ (Eq.S28). It comes:

$$\int d\mathbf{r} \sum_{\mathbf{u}} U_c^*(\mathbf{u}) H_{\text{out}}(\mathbf{u}, \mathbf{r}) T_0(\mathbf{u}, \mathbf{r} - \mathbf{r}_{\text{in}}) \gamma(\mathbf{r}) H_{\text{in}}(\mathbf{r}, \mathbf{r}_{\text{in}}) = H_{\text{in}}(\mathbf{r}_{\text{in}}, \mathbf{r}_{\text{in}}) \gamma(\mathbf{r}_{\text{in}})$$

This last equality is valid only and only if

$$\sum_{\mathbf{u}} U_c^*(\mathbf{u}) H_{\text{out}}(\mathbf{u},\mathbf{r}) T_0(\mathbf{u},\mathbf{r}-\mathbf{r}_{\text{in}}) = \delta(\mathbf{r}-\mathbf{r}_{\text{in}}) \tag{S43}$$

which, under the matrix formalism, can be rewritten as

$$(\mathbf{U_c} \circ \mathbf{T_0})^\dagger \mathbf{T} = \mathbb{I} \tag{S44}$$

The matrix $\hat{\mathbf{T}} = (\mathbf{U_c} \circ \mathbf{T_0})$ is an estimator of the transmission matrix $\mathbf{T}$. The application of its transpose conjugate, $\hat{\mathbf{T}}^\dagger$ enables a perfect compensation for the aberrations contained in the transmission matrix $\mathbf{T}$. To obtain a diffraction-limited image of the object, the matrix $\hat{\mathbf{T}}^\dagger$ should be directly applied to the output of the matrix $\mathbf{R}$ (Eq.12 of the accompanying paper). This operation leads to a focused matrix $\mathbf{R_F}$ whose coefficients can be expressed as

$$R_F(\mathbf{r}_{\text{out}},\mathbf{r}_{\text{in}}) = \gamma(\mathbf{r}_{\text{out}}) H_{\text{in}}(\mathbf{r}_{\text{out}},\mathbf{r}_{\text{in}}) \tag{S45}$$

This matrix consists in an Hadamard product between the reflectivity of the focal plane at its output and the input focusing matrix. In other words, aberrations are corrected at the output but subsists at the input. Hence the resulting confocal image built from the diagonal of $\mathbf{R_F}$ suffers from the same issue:

$$\mathcal{I}(\mathbf{r}_{\text{out}}) = R_F(\mathbf{r}_{\text{out}},\mathbf{r}_{\text{out}}) = \gamma(\mathbf{r}_{\text{out}}) H_{\text{in}}(\mathbf{r}_{\text{out}},\mathbf{r}_{\text{out}}) \tag{S46}$$

It is a relying estimator of the object's reflectivity $\gamma(\mathbf{r}_{\text{out}})$, but modulated by the amplitude and phase of the input illumination $H_{\text{in}}(\mathbf{r}_{\text{out}},\mathbf{r}_{\text{out}})$. To reduce this detrimental effect on the image contrast, one can consider a full-field image integrated over all input focusing beams (see Eq. 14 of the accompanying paper) or an adaptive confocal image integrating over a numerical pinhole (see Eq.18 of the accompanying paper). This integration over $\mathbf{r}_{\text{in}}$ allows us to smooth the modulation of the image induced by the input focusing beams.

S3.4 Finite size of the input PSF

All these theoretical developments have been made by considering a point-like input focused beam. This is, of course, not true in reality. The input focusing beam gives rise to a virtual coherent reflector of finite size δ_{in}. The issue we want to address is the impact of this size on the SVD of $\mathbf{D}$. Assuming incoherent input focusing beams (Eq. S2), Eq. S32 can be rewritten as follows in the isoplanatic limit (Eqs. S5-S6):

$$C_D(\mathbf{r}_{\text{in}}, \mathbf{r'}_{\text{in}}) \propto \left(\int d\mathbf{r} \gamma(\mathbf{r}) H_{\text{in}}(\mathbf{r} - \mathbf{r}_{\text{in}}) \right) \times \left(\int d\mathbf{r'} \gamma(\mathbf{r'}) H_{\text{in}}(\mathbf{r'} - \mathbf{r'}_{\text{in}}) \right)^*, \tag{S47}$$

By confronting this last equation with the eigenvalue decomposition of Eq. S39, it turns out that the distortion matrix $\mathbf{D}$ is of rank 1 and that its input singular vector $\mathbf{V_1}$ can be expressed as

$$V_1(\mathbf{r}_{\text{in}}) = \int d\mathbf{r} \gamma(\mathbf{r}) H_{\text{in}}(\mathbf{r} - \mathbf{r}_{\text{in}}) = [\gamma \circledast H_{\text{in}}](\mathbf{r}_{\text{in}}). \tag{S48}$$

where the symbol $\circledast$ stands for the convolution product. Albeit independent from output aberrations, $\mathbf{V_1}$ is nevertheless a convolution product between the object's reflectivity and the input PSF H_{in} (see Fig 2C of the accompanying paper). The output singular vector $\mathbf{U_1}$ can be deduced from $\mathbf{V_1}$ through the following matrix product:

$$\sigma_1 \mathbf{U_1} = \mathbf{D} \mathbf{V_1}. \tag{S49}$$

Injecting Eq. S10 and Eq. S48 into this last equation yields the following expression for the coefficients of $\mathbf{U_1}$

$$\sigma_1 \mathbf{U_1}(\mathbf{u}_{\text{out}}) = \hat{H}_{\text{out}}(\mathbf{u}_{\text{out}}) \int d\mathbf{r} \int d\mathbf{r'} \sum_{\mathbf{r}_{\text{in}}} T_0(\mathbf{u}_{\text{out}}, \mathbf{r} - \mathbf{r}_{\text{in}}) \gamma(\mathbf{r}) \gamma(\mathbf{r'}) H_{\text{in}}(\mathbf{r} - \mathbf{r}_{\text{in}}) H_{\text{in}}(\mathbf{r'} - \mathbf{r}_{\text{in}})$$

For a large number of resolution cells in the FOI, $\mathbf{U_1}$ will converge towards its ensemble average, such that

$$\sigma_1 \mathbf{U_1}(\mathbf{u}_{\text{out}}) = \hat{H}_{\text{out}}(\mathbf{u}_{\text{out}}) \int d\mathbf{r} \int d\mathbf{r'} \sum_{\mathbf{r}_{\text{in}}} T_0(\mathbf{u}_{\text{out}}, \mathbf{r} - \mathbf{r}_{\text{in}}) \gamma(\mathbf{r}) \gamma(\mathbf{r'}) \left\langle H_{\text{in}}(\mathbf{r} - \mathbf{r}_{\text{in}}) H_{\text{in}}(\mathbf{r'} - \mathbf{r}_{\text{in}}) \right\rangle$$

In a strong aberration regime (Eq. S2), the last equation can be rewritten as follows

$$\sigma_1 \mathbf{U_1}(\mathbf{u}_{\text{out}}) = \hat{H}_{\text{out}}(\mathbf{u}_{\text{out}}) \int d\mathbf{r} |\gamma(\mathbf{r})|^2 \sum_{\mathbf{r}_{\text{in}}} T_0(\mathbf{u}_{\text{out}}, \mathbf{r} - \mathbf{r}_{\text{in}}) \left\langle |H_{\text{in}}(\mathbf{r} - \mathbf{r}_{\text{in}})|^2 \right\rangle$$

Using the expression of the free-space transmission coefficients $T_0(\mathbf{u}_{\text{out}}, \mathbf{r}_{\text{in}})$ (Eq. 3), it finally turns out that

$$U_1(\mathbf{u}_{\text{out}}) \propto \hat{H}_{\text{out}}(\mathbf{u}_{\text{out}}) \left[\hat{H}_{\text{in}} * \hat{H}_{\text{in}} \right] (\mathbf{u}_{\text{out}}). \tag{S50}$$

and

$$\sigma_1 \propto \int d\mathbf{r} |\gamma(\mathbf{r})|^2. \tag{S51}$$

While the singular value σ_1 yields the object's reflectivity integrated over the associated isoplanatic patch (here the FOI), the vector $\mathbf{U_1}$ corresponds to the aberration output transmittance $\hat{H}_{\text{out}}$ modulated by the autocorrelation function of the aberration input transmittance $\hat{H}_{\text{in}}$ (see Fig 2C of the accompanying paper). This last term tends to limit the angular aperture of the singular vector $\mathbf{U_1}$ by the coherence angle of the input aberration $\hat{H}_{\text{in}}$. To circumvent that issue, the trick is to consider only the phase of the first singular vector $\mathbf{U_1}$. Indeed, if we make the realistic hypothesis of a real and positive autocorrelation function $\hat{H}_{\text{in}} * \hat{H}_{\text{in}}$, the normalized vector $\tilde{\mathbf{U}}_\mathbf{1}$ is then given by

$$\tilde{U}_1(\mathbf{u}_{\text{out}}) = \exp\left(j \arg\left\{U_1(\mathbf{u}_{\text{out}})\right\}\right) = \hat{H}(\mathbf{u}_{\text{out}}) \tag{S52}$$

A novel input vector $\tilde{\mathbf{V}}_\mathbf{1}$ can then be retrieved through the matrix product:

$$\tilde{\mathbf{U}}_\mathbf{1}^\dagger \mathbf{D} = \hat{\mathbf{V}}_\mathbf{1}. \tag{S53}$$

Injecting the expression of $\tilde{\mathbf{U}}_\mathbf{1}$ (Eq. S52) and $\mathbf{D}$ (Eq. S10), the following expression can be retrieved for $\hat{\mathbf{V}}_\mathbf{1}$ in the isoplanatic limit:

$$\hat{V}_1(\mathbf{r}_{\text{in}}) = H_{\text{in}}(\mathbf{r}_{\text{in}}, \mathbf{r}_{\text{in}}) \gamma(\mathbf{r}_{\text{in}}) \tag{S54}$$

If we compare this last equation with Eq. S48, the normalization of $\mathbf{U_1}$ allows us to virtually reduce the size of the input focusing beam (see Fig 2D of the accompanying paper). The matrix $\hat{\mathbf{T}} = (\tilde{\mathbf{U}}_\mathbf{1} \circ \mathbf{T_0})$ is then a satisfying estimator of the transmission matrix $\mathbf{T}$ in the isoplanatic limit. The application of its transpose conjugate, $\hat{\mathbf{T}}^\dagger$, allows a perfect compensation for the aberrations contained in the transmission matrix $\mathbf{T}$. A diffraction-limited image of the object can be obtained by applying the matrix $\hat{\mathbf{T}}^\dagger$ to the output of matrix $\mathbf{R}$ (Eq. 12).

S3.5 General case

In the general case (*i.e* beyond the isoplanatic limit), the same method can be employed to virtually reduce the size of the focal spot over each IM. The corresponding singular vectors should be normalized: $\tilde{\mathbf{U}}_\mathbf{p} = \exp\left(j\arg\left\{\mathbf{U}_\mathbf{p}\right\}\right)$. The application of their transpose conjugate to the $\mathbf{R}$-matrix should lead to an optimal aberration correction over each IM at the output. One open question is whether these output singular vectors can be combined coherently or not, such that $\tilde{\mathbf{U}}_\mathbf{c} = \sum_p \tilde{\mathbf{U}}_\mathbf{p}$. In the present work, this coherent combination does not provide better results than an incoherent summation of each IM image $\mathcal{I}_p$ (Eq.20). This is because an incoherent sum of $\mathbf{R_F}$-matrix coefficients at the input is required to smooth the modulation of the image by H_{in} (Eqs.14-18).

Supplementary Figures

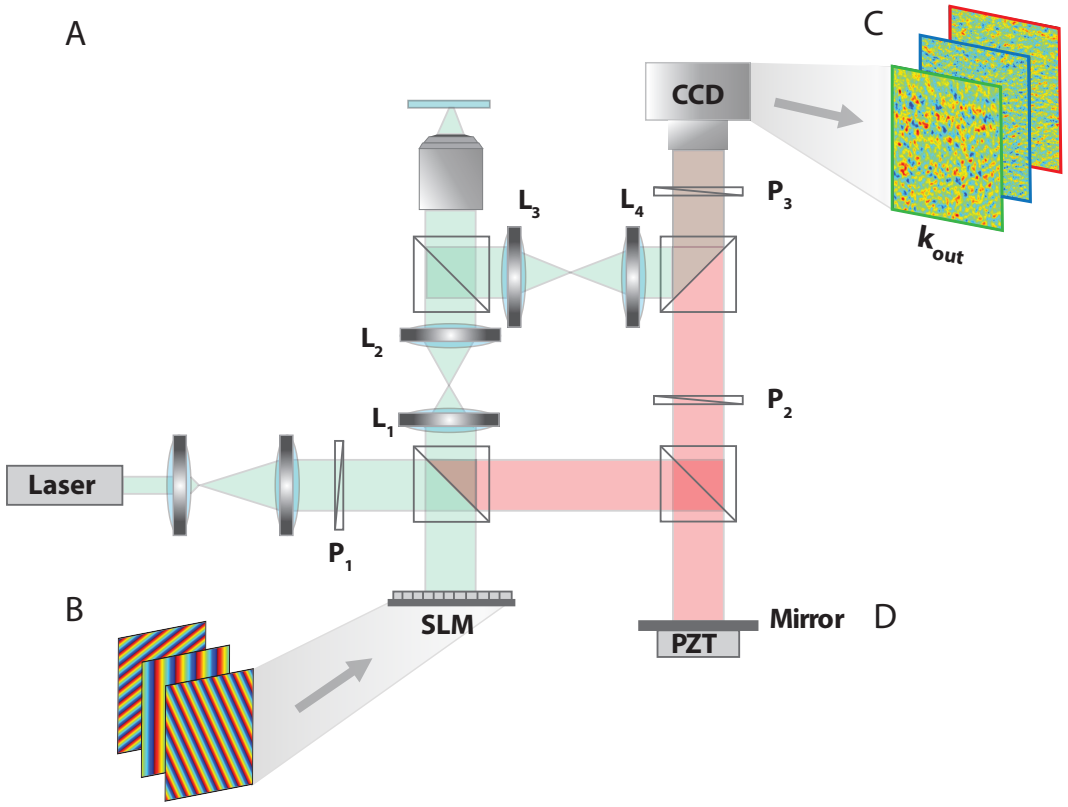

Figure S1: **Measuring the time-gated reflection matrix**. Experimental set up: P: polarizer, MO: microscope objective, BS: beam splitter, PBS: polarized beam splitter, SLM : spatial light modulator, PZT: piezo phase shifter, M: Mirror. A femtosecond laser beam (center wavelength: 810 nm, bandwidth: 40 nm) is shaped by an SLM acting as a diffraction grating. A set of incident plane waves is thus emitted from the SLM and focused at a different position in the focal plane of an immersion MO (NA=0.8). The backscattered wave-field is collected through the same MO and interferes with a reference beam on a CCD camera. The latter one is conjugated with the back focal plane of the MO. The amplitude and phase of the wave-field is recorded by phase shifting interferometry (*20*). The time of flight t is controlled by the length of the interferometric arm and is matched with the position of the focal plane. For each input focusing point $\mathbf{r}_{\text{in}}$, a reflected wave-field is recorded in the pupil plane and stored along a column vector in the matrix $\mathbf{R}) = [R(\mathbf{u}_{\text{out}}, \mathbf{r}_{\text{in}})]$.

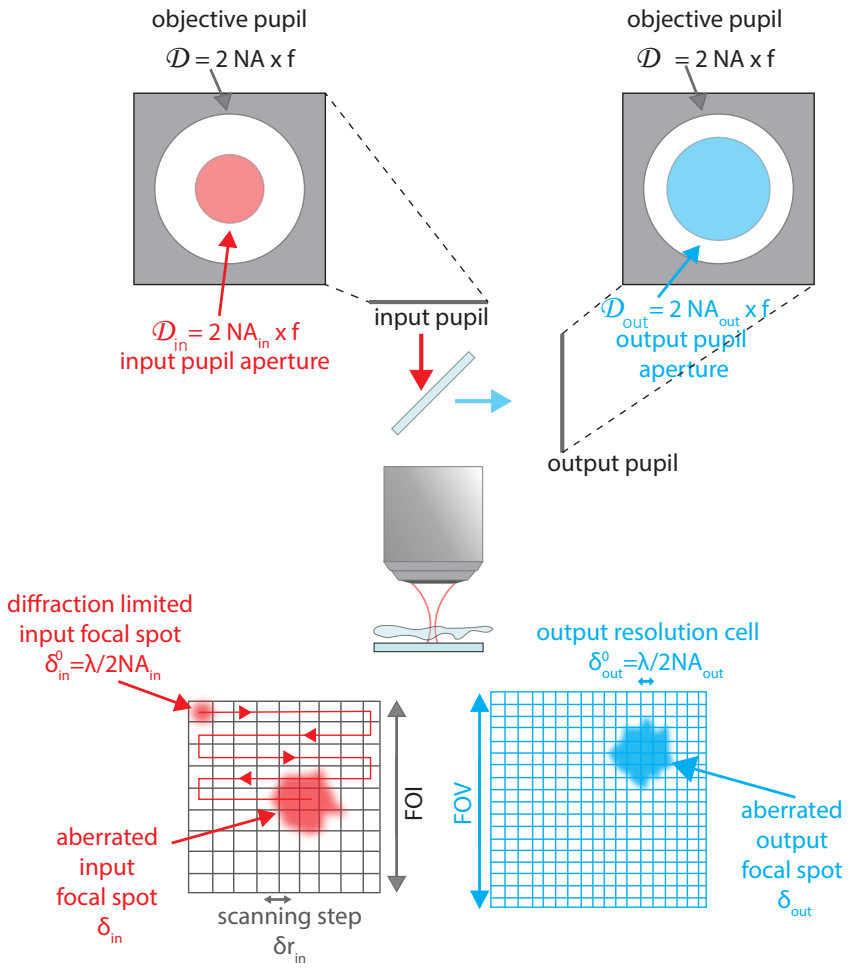

Figure S2: **Conjugation relationships between the pupil, focal and imaging planes**. The distortion matrix connects the focal plane of the MO with the output pupil plane. This figure illustrates the various parameters involved in the different planes of the system. Both input and output pupil planes are ultimately limited by the MO edges. The input pupil $\mathcal{D}_{\text{in}}$ is even more limited because the illumination beam underfills the objective pupil $\mathcal{D}$. It results in a reduced NA denoted NA_{in}. In turn, the size of the input focal spot in the image plane is given by $\delta^0_{\text{in}} = \lambda/2\text{NA}_{\text{in}}$ if there is no aberration and δ_{in} in the general case. In this focal plane, the field-of-illumination depends on the scanning step (spatial sampling), denoted as δr_{in}, and the number of measurements N_{in}. In reflection, the output pupil $\mathcal{D}_{\text{out}}$ is also smaller than the total objective pupil $\mathcal{D}$ due to the limited surface of the detector but larger than the input pupil $\mathcal{D}_{\text{in}}$. The resolution of the image is thus governed by the output resolution cell $\delta^0_{\text{out}} = \lambda/2\text{NA}_{in}$.

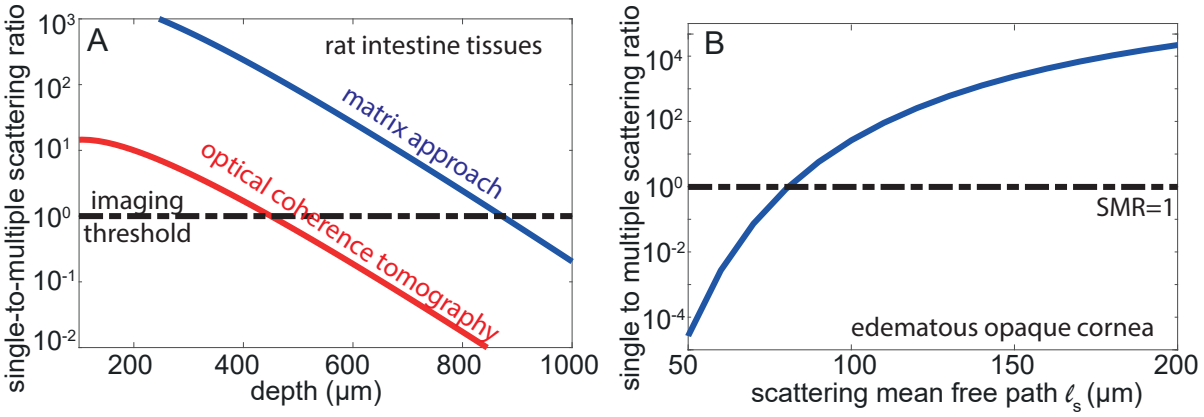

Figure S3: **Predicting the single-to-multiple scattering ratio in biological tissues.** (**A**) SMR as a function of depth for the imaging experiment through the rat intestinal tissue (see Figs. 1 and 3). The red curve (before aberration correction) is plotted for a Strehl ratio $\mathcal{S} = 3 \times 10^{-3}$, while the blue curve (after matrix correction) corresponds to $\mathcal{S} = 1.1 \times 10^{-2}$. The detection threshold yields an imaging depth limit of $\sim$ 450 μm for conventional OCT and 900 μm for our matrix approach. (**B**) SMR as a function of the scattering mean free path ℓ_s for the cornea imaging experiment (see Fig. 5). A SMR of 1 is obtained for a scattering mean free path $\ell_s \sim$ 80 μm. In both panels, the theoretical curves are built by considering the model described in Ref. (*38*) and the experimental parameters described in the paper. Note also that the y-axis is in log-scale.

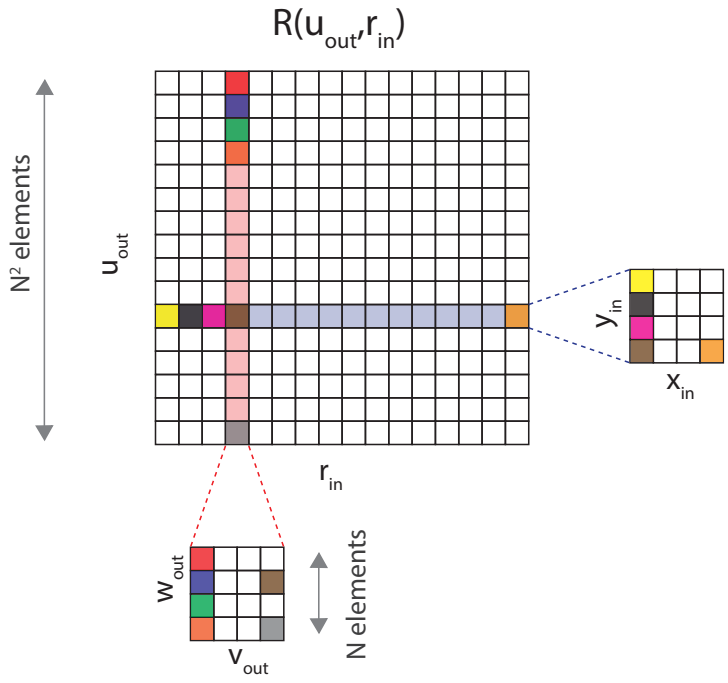

Figure S4: **Building the reflection matrix R**. For each focused illumination at $\mathbf{r}_{\text{in}} = (x_{\text{in}}, y_{\text{in}})$, the reflected wave-field $\psi_{\mathbf{r}_{\text{in}}}(v_{\text{out}}, w_{\text{out}})$ is recorded in the pupil plane by each pixel of the CCD camera whose position is denoted by the vector $\mathbf{u}_{\text{out}} = (v_{\text{out}}, w_{\text{out}})$. Each wave-field is concatenated and stored along a column vector. This set of column vectors forms the reflection matrix $\mathbf{R} = [R(\mathbf{u}_{\text{out}}, \mathbf{r}_{\text{in}})]$, such that $R(\mathbf{u}_{\text{out}}, \mathbf{r}_{\text{in}}) = \psi_{\mathbf{r}_{\text{in}}}(v_{\text{out}}, w_{\text{out}})$.

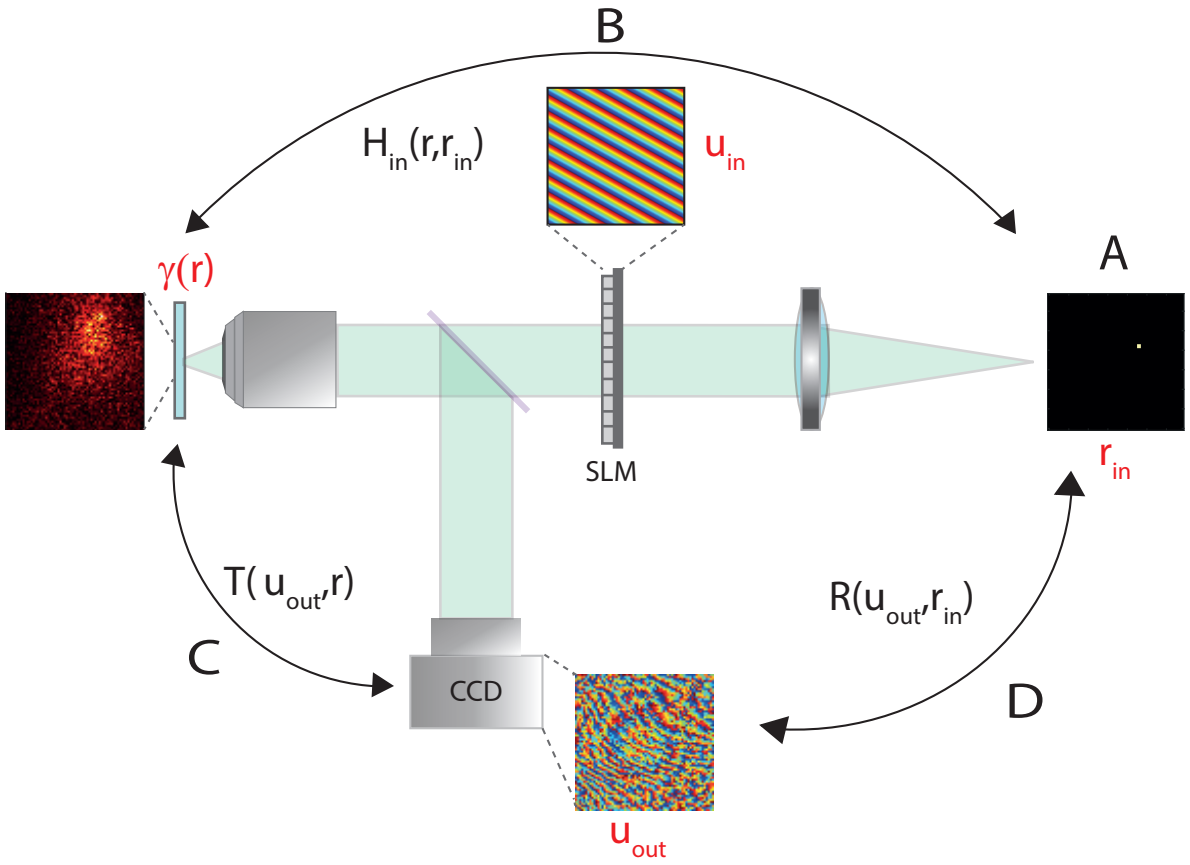

Figure S5: **Modeling light propagation from the virtual source plane to the output pupil plane.** The reflection matrix $\mathbf{R}$ contains the impulse responses $R(\mathbf{u}_{\text{out}}, \mathbf{r}_{\text{in}})$ between each virtual source point $\mathbf{r}_{\text{in}}$ and each CCD pixel $\mathbf{u}_{\text{out}}$ in the output pupil plane. (**A**) The virtual source point $\mathbf{r}_{\text{in}}$ is produced by each transverse mode shaped by the SLM in the input pupil plane. (**B**) The propagation between the virtual source plane and the focal plane of the MO can be modelled by the input focusing matrix $\mathbf{H}_{\text{in}} = [H_{\text{in}}(\mathbf{r}, \mathbf{r}_{\text{in}})]$ whose columns correspond to each input focal spot in the sample plane for each incident focusing point $\mathbf{r}_{\text{in}}$. (**C**) The return trip of the wave from the sample to the CCD camera is modeled by the transmission matrix $\mathbf{T} = [T(\mathbf{u}_{\text{out}}, \mathbf{r})]$ that connects each point $\mathbf{r}$ in the focal plane to each pixel $\mathbf{u}_{\text{out}}$ of the CCD camera. (**D**) Finally, based on these propagation matrices and the sample reflectivity matrix $\mathbf{\Gamma}$, the reflection matrix $\mathbf{R}$ can be simply expressed as the matrix product of these three matrices (Eq.1).

Supplementary tables

variable	definition
λ	wavelength
n	optical index
g	anisotropy factor
ℓ_s	scattering mean free path
L	thickness of the scattering layer
d	distance between the aberrating layer and the focal plane
f	focal length of the microscope objective
Ω	size of the field-of-illumination
$\mathbf{r}_{\rm in}$ / $\mathbf{r}_{\rm out}$	position vector in the input focusing / output pupil planes
$\mathbf{r}$	position vector in the focal plane of the microscope objective
$\mathbf{u}_{\rm out}$	position vector in the output pupil plane
$N_{\rm in}$ / $N_{\rm out}$	number of input focusing beams / pixels in the output pupil plane
$\mathcal{D}_{\rm in}$ / $\mathcal{D}_{\rm out}$	input / output pupil aperture
$\mathrm{NA}_{\rm in}$ / $\mathrm{NA}_{\rm out}$	input / output numerical aperture
$\delta r_{\rm in}$ / $\delta u_{\rm out}$	spatial sampling in the input focusing / output pupil planes
$\delta_{\rm in}$ / $\delta_{\rm out}$	characteristic width of the input/output point spread functions
$\delta^0_{\rm in}$ / $\delta^0_{\rm out}$	diffraction limit resolution at input/ouput
r_P / r_F	correlation length of the reflected wave-field in the output pupil / input focusing plane
d_P / d_F	correlation length of the distorted wave-field in the output pupil / input focusing plane
ℓ_γ	charateristic correlation length of the sample's reflectivity
ℓ_c	characteristic size of an isoplanatic patch
M_D / N_D	number of independent speckle grains for $\mathbf{D}$ in the input focusing / output pupil planes
M_R / N_R	number of independent speckle grains for $\mathbf{R}$ in the input focusing / output pupil planes
$\mathcal{S}_0$ / $\mathcal{S}_p$ / $\mathcal{S}'_p$	Strehl ratios: initial /final / weighted values
σ_p / $\tilde{\sigma}_p$	singular values of $\mathbf{D}$: raw / normalized
$\mathcal{H}(\tilde{\sigma}_p)$	Shannon entropy of singular values
SMR	single-to-multiple scattering ratio

Table S1: **Glossary of the variables used in this study.**

matrix	definition
$\mathbf{R} = [R(\mathbf{u}_{\rm out}, \mathbf{r}_{\rm in})]$	dual reflection matrix
$\mathbf{R_0} = [R_0(\mathbf{r}_{\rm out}, \mathbf{r}_{\rm in})]$	focused reflection matrix built from $\mathbf{T_0}$
$\mathbf{R_p} = [R_p(\mathbf{r}_{\rm out}, \mathbf{r}_{\rm in})]$	focused reflection matrix built from $\hat{\mathbf{T}}_\mathbf{p}$
$\mathbf{R_F} = [R_F(\mathbf{r}_{\rm out}, \mathbf{r}_{\rm in})]$	focused reflection matrix built from $\hat{\mathbf{T}}$
$\mathbf{T} = [T(\mathbf{u}_{\rm out}, \mathbf{r})]$	transmission matrix
$\mathbf{T_0} = [T_0(\mathbf{u}_{\rm out}, \mathbf{r})]$	free-space transmission matrix
$\hat{\mathbf{T}} = [\hat{T}(\mathbf{u}_{\rm out}, \mathbf{r}_{\rm out})]$	estimator of the transmission matrix
$\hat{\mathbf{T}}_\mathbf{p} = [\hat{T}_p(\mathbf{u}_{\rm out}, \mathbf{r})]$	estimator of the transmission matrix built from $\mathbf{U_p}$
$\mathbf{\Gamma} = [\gamma(\mathbf{r})]$	sample's reflectivity matrix
$\mathbf{\Gamma_D} = [\gamma_D(\mathbf{r})]$	virtual scatterer reflectivity matrix
$\mathbf{H}_{\rm in} = [H_{\rm in}(\mathbf{r}, \mathbf{r}_{\rm in})]$	input focusing matrix
$\mathbf{D} = [D(\mathbf{u}_{\rm out}, \mathbf{r}_{\rm in})]$	distortion matrix
$\mathbf{U_p} = [U_p(\mathbf{u}_{\rm out})]$	output singular vector of $\mathbf{D}$
$\tilde{\mathbf{U}}_\mathbf{p} = [\tilde{U}_p(\mathbf{u}_{\rm out})]$	normalized output singular vector of $\mathbf{D}$
$\mathbf{V_p} = [V_p(\mathbf{r}_{\rm in})]$	input singular vector of $\mathbf{D}$
$\mathbf{B_R} = [B_R(\mathbf{u}_{\rm out}, \mathbf{u'}_{\rm out})]$	correlation matrix of $\mathbf{R}$ in the pupil plane
$\langle \mathbf{B_R} \rangle = [\mathcal{B}_R(\Delta\mathbf{u})]$	covariance matrix of $\mathbf{R}$ in the puil plane
$\mathbf{B_D} = [B_D(\mathbf{u}_{\rm out}, \mathbf{u'}_{\rm out})]$	correlation matrix of $\mathbf{D}$ in the pupil plane
$\langle \mathbf{B_D} \rangle = [\mathcal{B}_D(\Delta\mathbf{u})]$	covariance matrix of $\mathbf{D}$ in the pupil plane
$\mathbf{C_R} = [C_R(\mathbf{u}_{\rm out}, \mathbf{u'}_{\rm out})]$	correlation matrix of $\mathbf{R}$ in the focal plane
$\langle \mathbf{C_R} \rangle = [\mathcal{C}_R(\Delta\mathbf{r})]$	covariance matrix of $\mathbf{R}$ in the focal plane
$\mathbf{C_D} = [C_D(\mathbf{u}_{\rm out}, \mathbf{u'}_{\rm out})]$	correlation matrix of $\mathbf{D}$ in the focal plane
$\langle \mathbf{C_D} \rangle = [\mathcal{C}_D(\Delta\mathbf{r})]$	covariance matrix of $\mathbf{D}$ in the focal plane
$\hat{\mathbf{H}}_{\rm out} = [\hat{H}_{\rm out}(\mathbf{u}_{\rm out}, \mathbf{r})]$	aberration matrix
$\mathbf{F} = [F(\mathbf{r}, \mathbf{r}')]$	correlation matrix of $\hat{\mathbf{H}}_{\rm out}$ in the focal plane

Table S2: **Glossary of the matrices used in this study.**

REFERENCES AND NOTES

1. H. W. Babcock, The possibility of compensating astronomical seeing. *Publ. Astron. Soc. Pac.* **65**, 229–236 (1953).

2. R. Foy, A. Labeyrie, Feasibility of adaptive telescope with laser probe. *Astron. Astrophys.* **152**, L29–L31 (1985).

3. S. T. Thurman, J. R. Fienup, Correction of anisoplanatic phase errors in digital holography. *J. Opt. Soc. Am. A* **25**, 995–999 (2008).

4. A. E. Tippie, J. R. Fienup, Multiple-plane anisoplanatic phase correction in a laboratory digital holography experiment. *Opt. Lett.* **35**, 3291–3293 (2010).

5. M. J. Booth, M. A. Neil, R. Juškaitis, T. Wilson, Adaptive aberration correction in a confocal microscope. *Proc. Natl. Acad. Sci. U.S.A.* **99**, 5788–5792 (2002).

6. X. Tao, B. Fernandez, O. Azucena, M. Fu, D. Garcia, Y. Zuo, D. C. Chen, J. Kubby, Adaptive optics confocal microscopy using direct wavefront sensing. *Opt. Lett.* **36**, 1062–1064 (2011).

7. D. Débarre, E. J. Botcherby, T. Watanabe, S. Srinivas, M. J. Booth, T. Wilson, Image-based adaptive optics for two-photon microscopy. *Opt. Lett.* **34**, 2495–2497 (2009).

8. N. Ji, D. E. Milkie, E. Betzig, Adaptive optics via pupil segmentation for high-resolution imaging in biological tissues. *Nat. Methods* **7**, 141–147 (2010).

9. I. N. Papadopoulos, J.-S. Jouhanneau, J. F. Poulet, B. Judkewitz, Scattering compensation by focus scanning holographic aberration probing (f-sharp). *Nat. Photonics* **11**, 116–123 (2017).

10. M. Rueckel, J. A. Mack-Bucher, W. Denk, Adaptive wavefront correction in two-photon microscopy using coherence-gated wavefront sensing. *Proc. Natl. Acad. Sci. U.S.A.* **103**, 17137–17142 (2006).

11. B. Hermann, E. Fernández, A. Unterhuber, H. Sattmann, A. Fercher, W. Drexler, P. Prieto, P. Artal, Adaptive-optics ultrahigh-resolution optical coherence tomography. *Opt. Lett.* **29**, 2142–2144 (2004).

12. S. G. Adie, B. W. Graf, A. Ahmad, P. S. Carney, S. A. Boppart, Computational adaptive optics for broadband optical interferometric tomography of biological tissue. *Proc. Natl. Acad. Sci. U.S.A.* **109**, 7175–7180 (2012).

13. B. Judkewitz, R. Horstmeyer, I. M. Vellekoop, I. N. Papadopoulos, C. Yang, Translation correlations in anisotropically scattering media. *Nat. Phys.* **11**, 684–689 (2015).

14. F. J. Rigaut, B. L. Ellerbroek, R. Flicker, in *Adaptive Optical Systems Technology*, P. L. Wizinowich, Ed. (SPIE, 2000), pp. 432–441.

15. Z. Kam, P. Kner, D. Agard, J. W. Sedat, Modelling the application of adaptive optics to wide-field microscope live imaging. *J. Microsc.* **226**, 33–42 (2007).

16. R. D. Simmonds, M. J. Booth, Modelling of multi-conjugate adaptive optics for spatially variant aberrations in microscopy. *J. Opt.* **15**, 094010 (2013).

17. M. Minski, Microscopy apparatus. US patent 3013467 (1961).

18. M. R. Hee, E. A. Swanson, J. G. Fujimoto, J. A. Izatt, Femtosecond transillumination tomography in thick tissues. *Opt. Lett.* **18**, 1107–1109 (1993).

19. I. M. Vellekoop, A. P. Mosk, Focusing coherent light through opaque strongly scattering media. *Opt. Lett.* **32**, 2309–2311 (2007).

20. S. M. Popoff, G. Lerosey, R. Carminati, M. Fink, A. C. Boccara, S. Gigan, Measuring the Transmission Matrix in Optics: An Approach to the Study and Control of Light Propagation in Disordered Media. *Phys. Rev. Lett.* **104**, 100601 (2010).

21. S. M. Popoff, G. Lerosey, M. Fink, A. C. Boccara, S. Gigan, Image transmission through an opaque material. *Nat. Commun.* **1**, 81 (2010).

22. M. Kim, Y. Choi, C. Yoon, W. Choi, J. Kim, Q.-H. Park, W. Choi, Maximal energy transport through disordered media with the implementation of transmission eigenchannels. *Nat. Photonics* **6**, 583–587 (2012).

23. T. Cizmar, K. Dholakia, Exploiting multimode waveguides for pure fibre- based imaging. *Nat. Commun.* **3**, 1027 (2012).

24. I. N. Papadopoulos, S. Farahi, C. Moser, D. Psaltis, Focusing and scanning light through a multimode optical fiber using digital phase conjugation. *Opt. Express* **20** 10583–10590 (2012).

25. S. A. Alexandrov, T. R. Hillman, T. Gutzler, D. D. Sampson, Synthetic aperture fourier holographic optical microscopy. *Phys. Rev. Lett.* **97**, 168102 (2006).

26. S. M. Popoff, A. Aubry, G. Lerosey, M. Fink, A. C. Boccara, S. Gigan, Exploiting the time-reversal operator for adaptive optics, selective focusing, and scattering pattern analysis. *Phys. Rev. Lett.* **107**, 263901 (2011).

27. A. Badon, D. Li, G. Lerosey, A. C. Boccara, M. Fink, A. Aubry, Smart optical coherence tomography for ultra-deep imaging through highly scattering media. *Sci. Adv.* **2**, e1600370 (2016).

28. Y. Choi, T. R. Hillman, W. Choi, N. Lue, R. R. Dasari, P. T. C. So, W. Choi, Z. Yaqoob, Measurement of the time-resolved reflection matrix for enhancing light energy delivery into a scattering medium. *Phys. Rev. Lett.*,**111** 243901 (2013).

29. S. Jeong, Y.-R. Lee, W. Choi, S. Kang, J. H. Hong, J.-S. Park, Y.-S. Lim, H.-G. Park, W. Choi, Focusing of light energy inside a scattering medium by controlling the time-gated multiple light scattering. *Nat. Photonics* **12**, 277–283 (2018).

30. S. Kang, S. Jeong, W. Choi, H. Ko, T. D. Yang, J. H. Joo, J.-S. Lee, Y.-S. Lim, Q.-H. Park, W. Choi, Imaging deep within a scattering medium using collective accumulation of single-scattered waves. *Nat. Photonics* **9**, 253–258 (2015).

31. S. Kang, P. Kang, S. Jeong, Y. Kwon, T. D. Yang, J. H. Hong, M. Kim, K.-D. Song, J. H. Park, J. H. Lee, M. J. Kim, K. H. Kim, W. Choi, High-resolution adaptive optical imaging within thick scattering media using closed-loop accumulation of single scattering. *Nat. Commun.* **8**, 2157 (2017).

32. J.-L. Robert, M. Fink, Green's function estimation in speckle using the decomposition of the time reversal operator: Application to aberration correction in medical imaging. *J. Acoust. Soc. Am.* **123** 866–877 (2008).

33. J.-L. Robert, M. Fink, The time-reversal operator with virtual transducers: Application to far-field aberration correction. *J. Acoust. Soc. Am.* **124**, 3659–3668 (2008).

34. G. Osnabrugge, R. Horstmeyer, I. N. Papadopoulos, B. Judkewitz, I. M. Vellekoop, Generalized optical memory effect. *Optica* **4**, 886–892 (2017).

35. S. L. Jacques, Optical properties of biological tissues: A review. *Phys. Med. Biol.* **58**, R37–R61 (2013).

36. M. Born, E. Wolf, *Principles of Optics: Electromagnetic Theory of Propagation, Interference and Diffraction of Light* (CUP Archive, 1999).

37. J. Mertz, H. Paudel, T. G. Bifano, Field of view advantage of conjugate adaptive optics in microscopy applications. *Appl. Opt.* **54**, 3498–3506 (2015).

38. A. Badon, A. C. Boccara, G. Lerosey, M. Fink, A. Aubry, Multiple scattering limit in optical microscopy. *Opt. Express* **25**, 28914–28934 (2017).

39. V. N. Mahajan, Strehl ratio for primary aberrations: some analytical results for circular and annular pupils. *J. Opt. Soc. Am.* **72**, 1258–1266 (1982).

40. L. L. Campbell, Minimum coefficient rate for stationary random processes. *Inf. Control.* **3**, 360–371 (1960).

41. S. J. Roberts, W. Penny, L. Rezek, Temporal and spatial complexity measures for electroencephalogram based brain-computer interfacing. *Med. Biol. Eng. Comput.* **37**, 93–98 (1999).

42. R. G. Ghanem, R. D. Spanos, *Stochastic Finite Elements: A Spectral Approach* (Springer-Verlag, 1991).

43. J.-L. Robert, M. Fink, The prolate spheroidal wave functions as invariants of the time reversal operator for an extended scatterer in the fraunhofer approximation. *J. Acoust. Soc. Am.* **125**, 218–226 (2009).

44. A. Aubry, J. de Rosny, J.-G. Minonzio, C. Prada, M. Fink, Gaussian beams and legendre polynomials as invariants of the time reversal operator for a large rigid cylinder. *J. Acoust. Soc. Am.* **120**, 2746–2754 (2006).

45. R. Bocheux, P. Pernot, V. Borderie, K. Plamann, K. Irsch, Quantitative measures of corneal transparency, derived from objective analysis of depth-resolved corneal images, demonstrated with full-field optical coherence tomographic microscopy. *PLOS ONE* **14**, e0221707 (2019).

46. M. Bastiaans, Wigner distribution function and its application to first-order optics. *J. Opt. Soc. Am.* **69**, 1710–1716 (1979).

47. M. Kim, Y. Jo, J. H. Hong, S. Kim, S. Yoon, K.-D. Song, S. Kang, B. Lee, G. H. Kim, H.-C. Park, W. Choi, Label-free neuroimaging in vivo using synchronous angular scanning microscopy with single-scattering accumulation algorithm. *Nat. Commun.* **10**, 3152 (2019).

48. S. Yoon, H. Lee, J. H. Hong, Y.-S. Lim, W. Choi, Laser scanning reflection-matrix microscopy for label-free in vivo imaging of a mouse brain through an intact skull. arXiv:1910.04681 (2019).

49. A. Badon, G. Lerosey, A. C. Boccara, M. Fink, A. Aubry, Retrieving time-dependent green's functions in optics with low-coherence interferometry. *Phys. Rev. Lett.* **114**, 023901 (2015).

50. A. Badon, D. Li, G. Lerosey, A. C. Boccara, M. Fink, A. Aubry, Spatio-temporal imaging of light transport in highly scattering media under white light illumination. *Optica* **3**, 1160–1166 (2016).

51. W. Lambert, L. A. Cobus, T. Frappart, M. Fink, A. Aubry, Distortion matrix approach for ultrasound imaging of random scattering media. *Proc. Natl. Acad. Sci. U.S.A.*, (2020).

52. A. Badon, V. Barolle, A. C. Boccara, M. Fink, K. Irsch, A. Aubry, Towards characterization and compensation of loss of anterior segment transparency. *IEEE Transactions on Engineering in Medicine and Biology Conference (EMBC)* (IEEE, 2019).

53. V. Lauer, New approach to optical diffraction tomography yielding a vector equation of diffraction tomography and a novel tomographic microscope. *J. Microsc.* **205**, 165–176 (2002).

54. S. Shahjahan, A. Aubry, F. Rupin, B. Chassignole, A. Derode, A random matrix approach to detect defects in a strongly scattering polycrystal: How the memory effect can help overcome multiple scattering. *Appl. Phys. Lett.* **104**, 234105 (2014).

55. T. Blondel, J. Chaput, A. Derode, M. Campillo, A. Aubry, Matrix approach of seismic imaging: Application to the erebus volcano, Antarctica. *J. Geophys. Res. Solid Earth* **123**, 10936–10950 (2018).

56. T. Zhang, K. Unger, G. Maire, P. C. Chaumet, A. Talneau, C. Godhavarti, H. Giovannini, K. Belkebir, A. Sentenac, Multi-wavelength multi-angle reflection tomography. *Opt. Express* **26**, 26093–26105 (2018).

57. J.-L. Robert, Evaluation of green's functions in complex media by decomposition of the time reversal operator: Application to medical imaging and aberration correction, thesis, Universite Paris 7–Denis Diderot (2007).

58. M. Priestley, *Spectral Analysis and Time Series* (Academic Press, 1988).

59. J. W. Goodman, *Statistical Optics* (Wiley, 2000).

60. C. Prada, J.-L. Thomas, Experimental subwavelength localization of scatterers by decomposition of the time reversal operator interpreted as a covariance matrix. *J. Acoust. Soc. Am.* **114**, 235–243 (2003).

61. C. Prada, M. Fink, Eigenmodes of the time reversal operator: A solution to selective focusing in multiple-target media. *Wave Motion* **20**, 151–163 (1994).